Self-Strengthening Tape Junctions Inspired by Recluse Spider Webs

Ben H. Skopic,[1] Sean R. Koebley,[1] and Hannes C. Schniepp*[1]

[1] Applied Science Department, William & Mary, P.O. Box 8795, Williamsburg, VA, 23187-8795, USA.

*Lead contact: E-mail: schniepp@wm.edu

—Supplementary Information—

SI1 – Peeling Mode Failure

Peeling ensues when the junction buckles into the nestled conformation, as shown in Fig. S1. Figs. S1a and S1b show photographs from two different perspectives of the same junction, and Figs. S1c and S1d show the corresponding schematic representations. Here we develop a model to include the effect that the azimuthal junction angle, ϕ, has on the peeling of two intersecting tapes. A key difference between the peeling of a tape–tape junction with an azimuthal junction angle and current peeling models[S1,S2] is that our system does not have a simple rectangular contact geometry, thus geometric boundary conditions arise. The intersection of two tapes leads to the contact area of the junction (junction area) forming the rhombus $PACD$ (Fig. S1c). Peeling begins at point P with the peeling front oriented parallel to the longer bisecting diagonal of the rhombus AD and moves in the direction of the shorter bisecting diagonal, PC, as shown in Fig. S1c. The total peeling distance along the rhombus is PC and in Fig. S1c is split into l, the unpeeled length and l', the peeled length. Peeling a distance l' effectively elongates the specimen in the tensile direction by a length x, as shown in Fig. S1d. The maximum tensile length added when peeling completes and the two tapes separate is defined as x_{max}, which can be determined as follows:

$$x_{max} = 2w \tan\frac{\phi}{2},$$
(S1)

where ϕ is the junction angle and w is the width of the tape. As peeling progresses, the peeled area continuously increases, where the width of the peeling front first linearly increases, peaks when it is equal to the longer bisecting diagonal AD at $x = x_{max}/2$, then decreases symmetrically according to the shape of the rhombus. The peeled area changes with the width of the peeling front and can be expressed as a function of tensile displacement, x, as:

$$A(x) = \csc^2\left(\frac{\phi}{2}\right)\cot\left(\frac{\phi}{2}\right) \cdot \begin{cases} x^2 & 0 \leq x \leq \frac{x_{max}}{2} \\ 2\left(\frac{x_{max}}{2}\right)^2 - (x_{max} - x)^2 & \frac{x_{max}}{2} \leq x \leq x_{max} \end{cases}.$$
(S2)

We are now ready to determine the force due to peeling as a function of the tensile displacement x. Traditional peeling models relate the polar angle, θ, between the applied force F and the substrate to the

magnitude of the force at which peeling occurs.[S1] Thus, we need to determine the θ for our peeling system. In Figs. S1b and S1d, the junction area is oriented perpendicular with respect to the plane of the images, and the tapes move in the plane of the images during the peeling process. Therefore, the polar peeling angle θ relative to the substrate (or in this case, the complimentary tape) is 90°. This behavior is similar the T-peel test where the contact area between the two tapes peeled apart assumes a 90° orientation with respect to the pulling direction, so that the sample makes the shape of a "T". More advanced models treating the T-peel test have also considered the effect of gravity on the contact area, causing it to make an angle different from 90°.[S3] In our case, however, the junction area is not oriented perpendicular to the tensile direction, reducing the degree to which gravity orients it away from a perfect 90° angle. Therefore, we have neglected these gravitational effects and assumed $\theta = 90°$, for which it has been shown that the tapes experience no elastic extension.[S1,S4] In this case, all of the energy goes into separating the two tapes through peeling.
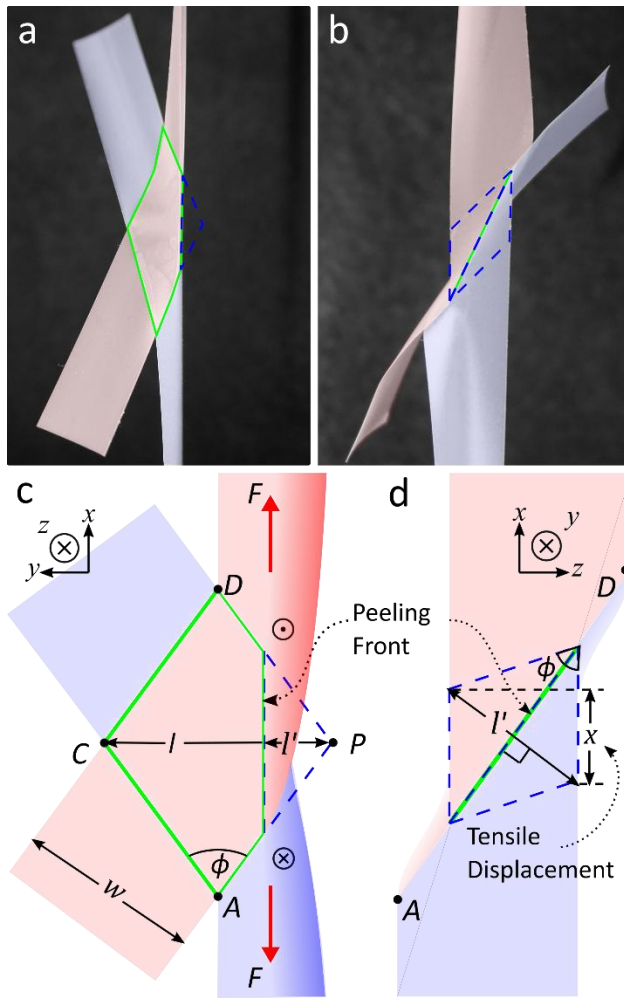

Fig. S1. Diagram for the nestled conformation featuring the rhombic contact geometry, related to Fig. 2c and Eqn. 2

(a) and (b) are false-colored photographs of the tape junction at two different perspectives; (b) is rotated 90° clockwise around the x-axis with respect to (a). (c) and (d) are schematics of the corresponding photographs above. According to the coordinate axes shown, (a) and (c) view the junction area from the z direction, featuring its originally rhombic shape (green outline, blue dashed line representing the area already peeled apart). (b) and (d) view the junction from the side (y direction). In the perspective shown in (a) and (c), the red tape lies on top of the blue tape. In (c) the bullseye on the top tape indicates that the darker region folds out of the page and the cross on the bottom tape indicates that it folds into the page.

The derivation of the peeling force of this system begins with the common energy–force relationship:

$$F = \frac{d}{dx} U,$$ (S3)

where x is the displacement in the direction of F and U is the work. In absence of any elastic energy contributions, this work is converted entirely into surface energy, γ:

$$\gamma = \frac{U}{A},$$ (S4)

where A is the new surface area created by separating two surfaces. Eqns. S3 and S4 can be combined to give:

$$F = \gamma \frac{d}{dx} A(x).$$ (S5)

Since $A(x)$ accounts for the changing width of the peeling front, eqn. S5 allows us to determine the peeling force as a function of the tensile displacement, x, of any peeling system when $\theta = 90°$, independent of the junction geometry. Therefore, by taking the derivative of eqn. S2 according to eqn. S5, we get the peeling force for our intersecting tapes:

$$F_p(x) = 2\gamma \csc^2\left(\frac{\phi}{2}\right)\cot\left(\frac{\phi}{2}\right) \cdot \begin{cases} x & 0 \le x \le \frac{x_{max}}{2} \\ (x_{max} - x) & \frac{x_{max}}{2} \le x \le x_{max} \end{cases}.$$ (S6)

This result is a triangular force profile that requires an infinitesimally small force to begin peeling because the initial width of the peeling front is infinitesimally small. This is different from the peeling models with a fixed width of the peeling front which peels at a constant force once a minimum force threshold is met.

To get the energy of peeling, we take the integral of eqn. S6 according to eqn. S3:

$$U_p(x) = \int_0^{x_{max}} F_p(x) dx$$ (S7)

$$U_p(x) = \gamma \csc^2\left(\frac{\phi}{2}\right)\cot\left(\frac{\phi}{2}\right) \cdot \begin{cases} x^2 & 0 \le x \le \frac{x_{max}}{2} \\ 2\left(\frac{x_{max}}{2}\right)^2 - (x_{max} - x)^2 & \frac{x_{max}}{2} \le x \le x_{max} \end{cases}.$$ (S8)

SI2 – Elastic Strain

If a particular junction has a junction angle that is in region III and the junction buckles into the locked conformation or is in either regions I or II, it will experience elastic strain. With respect to the distribution of stresses and strains, the junction has mirror symmetry with respect to a line through points C and P in Fig. S2a. Correspondingly, it suffices to only determine stresses and strains to the left of this line. Based on the particular geometry of the junction, the side of the junction next to the green lines is longer and has excess material, whereas the side next to the pink lines is shorter. In the configuration shown in Fig. S2c, only the pink line is oriented in the tensile direction and, therefore, is the only portion of the material being strained. As the tensile load increases and the areas near the pink line get increasingly strained, the length difference with the green line is reduced, and areas closer to the green line become strained as well. As more material is strained, the region of the junction that is strained becomes planar while the unstrained region remains relaxed in the buckled conformation. The dividing line between strained and unstrained regions of the asymmetrically loaded junction is indicated as a black, dashed line in Fig. S2a. This dividing line is separated by a distance h from the pink line, which increases as the straining proceeds. Based on the position of the dividing line, we consider different regions of the junction, which we quantify using a dedicated system of variables x_i ($i = 0,1,2,3$), as depicted in Fig. S2a, where

$$x_0 = w \cot \phi, \tag{S9}$$

$$x_1 = (w - h) \cot \phi \qquad x_0 \le x_1 \le 0 \tag{S10}$$

$$x_2 = h \cot \phi \qquad 0 \le x_2 = x_0 - x_1 \le x_0 \tag{S11}$$

$$x_3 = h \tan \frac{\phi}{2} \qquad 0 \le x_3 \le w \tan \frac{\phi}{2} \tag{S12}$$

In addition to the material in the vicinity of the junction area, the tape outside of this region, b, contributes to the load-dependent extension of the sample. It is

$$b = \frac{\beta}{2} - x_0, \tag{S13}$$

where β is the total sample length, which we kept constant for all junction angles ϕ. With increasing junction angle, b increases and x_0 decreases.
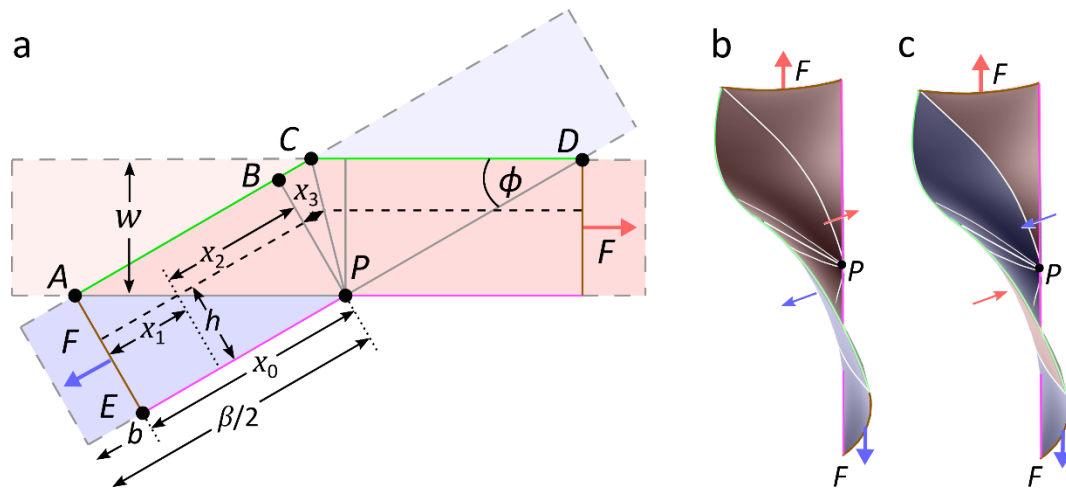

Fig. S2. Schematic Diagram for the Elastic Model, related to Fig. 2D and Eqn. 3

(a) Tape–tape junction schematic with ϕ = 30° describes how the elastic model is derived. The red and blue shadings represent the top and bottom tapes, respectively. (b) Depiction of junction area buckling into the "nestled" shape, allowing peeling. (c) "Locked" conformation leading to the cusp and elastic strain. The regions outlined with gray, dashed lines in (a) are not shown in (b) or (c).

In general terms, the derivation of the elastic strain on the rhombic junction begins with the definition of stress, σ, for a linearly elastic material with Young's modulus E:

$$\sigma_e = E\epsilon. \tag{S14}$$

Using the definitions of stress and strain, ϵ, respectively, we get:

$$\frac{F_e}{A} = E \frac{x}{L_0}, \tag{S15}$$

where x is the displacement in the tensile direction, L_0 is the unstretched length of the material, and A is the cross-sectional area of the material being strained. We can solve eqn. S15 for F to get:

$$F_e = E \frac{x}{L_0} tw, \tag{S16}$$

where A was substituted for the width, w, and thickness, t, of a rectangular cross-section. In the case of our angled junction, the stresses and strains are unevenly distributed over the junction, and therefore, we break the cross-

sectional area into infinitesimal force components dF along h, with width dh. In this geometry, each infinitesimal element has a different initial unstretched length, L_0 (having a contribution from each segment represented by b and the x_i variables), and a different thickness (the regions represented by variables x_2 and x_3 are two tape layers thick and the x_1 and b regions are a single layer thick). Thus, the force on each infinitesimal element can be expressed as

$$dF = E\frac{x}{L_0(x_i,b)}t_{avg}dh, \tag{S17}$$

where t_{avg} is the average thickness of the element across the four segments b and x_i. Finally, we can express L_0 and t_{avg} through the variables b and x_i as defined in Eqns. S9–S13:

$$dF = E\left[\frac{x}{2(x_1(x,h)+x_2(x,h)+x_3(x,h)+b)}\right]t\left[1+\frac{x_2(x,h)+x_3(x,h)}{x_1(x,h)+b}\right]dh, \tag{S18}$$

where we obtain t_{avg} by considering the ratio of regions with 2 layers (x_2+x_3) over the sections with one layer (x_1+b). The factor of two in the initially unstretched length accounts for the other half of the junction, subject to mirror symmetry about line PC. Substituting the definitions for each variable into eqn. S18 and simplifying, we find that the force of the infinitesimal element is proportional to the total extension x, as expected:

$$dF = -Etx\frac{\tan\phi}{2h-\beta\tan\phi}dh. \tag{S19}$$

To get the total force, we integrate all infinitesimal elements along h using eqn. S19, where we limit the range of the integral to only consider the elements that get strained:

$$F_e = \int_0^{2x\cot\frac{\phi}{2}} -Etx\frac{\tan\phi}{2h-\beta\tan\phi}dh \qquad\qquad 0\leq x\leq\tan\frac{\phi}{2}. \tag{S20}$$

For a given extension x, only the infinitesimal elements below the black, dashed line in Fig. S2a get strained. Although each infinitesimal element is treated as a linear-elastic material, the overall stress–strain behavior of the junction is non-linear for small strains because the upper boundary of the integral in eqn. S20 is a function of x, as discussed in more detail below.

For larger strains, eqn. S20 predicts the slope of the elastic force to exceed the modulus of the single layered tape E because the junction area is two tape layers thick. However, we observe that the slope of the elastic force becomes approximately linear and equal to the modulus of the single-layered tape as shown in Fig. S3. As the extension grows, the cost to strain the growing two-layered region increases, causing more single-layered material to be strained outside of the junction area instead such that the overall stress–strain behavior is approximately linear. We define the tensile displacement x at which this transition into the linear regime occurs as α, which is different for every junction angle. The complete elastic model as a function of x is:

$$F_e(x) = \begin{cases} -\frac{1}{2}Etx\tan\phi\ln\left|\frac{2x}{\beta\tan\left(\frac{\phi}{2}\right)\tan\phi}-1\right| & 0\leq x\leq\alpha \\ wE(x-\alpha)+F_e(\alpha) & x\geq\alpha \end{cases}. \tag{S21}$$

By definition, α is the tensile displacement at which the slope of $F_e(x)$ reaches the slope of a single straight ribbon, wE, and can be determined accordingly. This is done by taking the derivative of each part of eqn. S21 and setting both parts equal. This results in the following transcendental equation:

$$\exp\left(\frac{2x}{\beta\tan\frac{\phi}{2}-2x}-\frac{2w}{t\tan\phi}\right) = \frac{2x}{\beta\tan\frac{\phi}{2}\tan\phi}. \tag{S22}$$

Thus, the numerical solution to eqn. S22 determines where $x = \alpha$ for each ϕ.

To get the elastic energy as a function of the tensile displacement, the integral of eqn. S21 is taken according to eqn. S3:

$$U_e(x) = \int_0^x F_e(x)dx. \tag{S23}$$

This integral can only be solved numerically due to the x inside the natural logarithm.

SI3 – Assessment of Assumptions

Eqn. S21 provides a solution to the elastic strain on this tape–tape junction that is in agreement with all our experimental data. Our model expands the traditional treatment of peeling and uses the same assumptions as the pertinent literature (see discussion in SI1). In addition, there are three key assumptions limiting the model, in principle. First, we assume that the material is linear-elastic, as already discussed in the manuscript and further below. Second, the model assumes that shear forces from within the tapes and in between the two tapes can be neglected. The former can be neglected based on the geometry of the junction, the latter are negligible because the tapes are thin.[S5,S6] The third assumption is that the junction is clamped symmetrically, i.e. the distance of the clamping points from the junction are identical on both sides of the junction area. This assumption means that point P of the junction is at $\beta/2$, and correspondingly, forces are symmetric on both sides of the junction. The loops in the recluse's looped metastructure are evenly spaced at 200 loops/cm.[S7] Therefore, this assumption is fully met for each individual loop. For the tape experiments, human error limited the precision of loading each sample into the tensile tester. The corresponding deviation from a perfectly symmetrical sample loading was ±3 mm. This amount of experimental error is not a significant deviation from our assumptions and does not affect the conclusions of the manuscript.
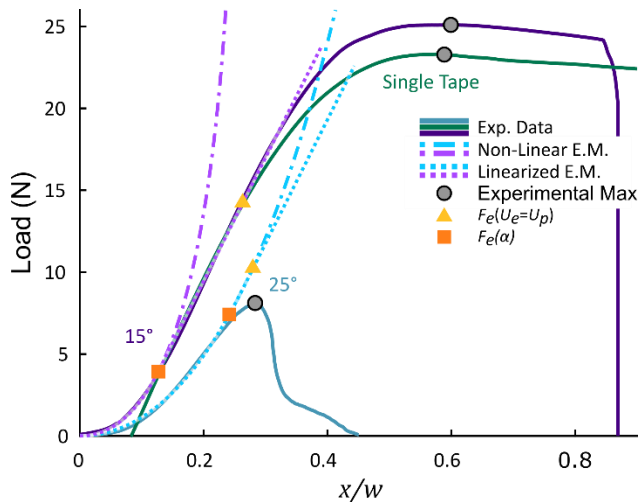

Fig. S3. Motivation for Linearization of Elastic Model, related to Fig. 3 and Eqn. 3

Experimental tensile data normalized by the width w from $\phi = 15°$ and $\phi = 25°$ samples (solid lines). Also plotted are these two samples' corresponding elastic models (E.M.) (dashed-dotted lines) as described by eqn. S20, and the linearized E.M. (dotted lines) as described by eqn. S21. The dark green line represents single tape data, which was shifted horizontally to align with the linear region (orange square) of the $\phi = 15°$ sample and shows that the linearization of eqn. S21 is a good approximation.

To assess the linear range of the material used in our experiment, we provide the solid green curve in Fig. S3, showing the tensile behavior of a single tape. Taking into account the horizontal offset at which this curve is

shown, the yield point of the tape is at $x/w \approx 0.18$, where the second derivative of the strain becomes negative. As our model does not account for any non-linear behavior, it is only strictly correct for strains up to $x/w \approx 0.18$. However, in Fig. S3, the ϕ = 15° sample continues behaving linearly beyond $x/w \approx 0.18$, until $x/w \approx 0.22$. The likely reason for this lies in the geometry of this system, where most areas of the junction feature a local strain significantly smaller than x/w, due to the extra material in the buckled region. Correspondingly, the non-linearity manifests very slowly and only at larger strains. However, materials with different non-linear behavior may exhibit a different range of the linear region. For the case of the recluse spider silk, the linear properties can be viewed with the blue curve in Fig. 2a. The recluse silk exhibits approximately linear elastic behavior for the entirety of it's mechanical response. For these reasons, we are confident in our linear elastic assumption for Eqn. S21 is accurate for both the Scotch® tape used in the single junction experiment and the looped metastructure of the recluse spider.

SI4 – Pre-Buckling Parameters

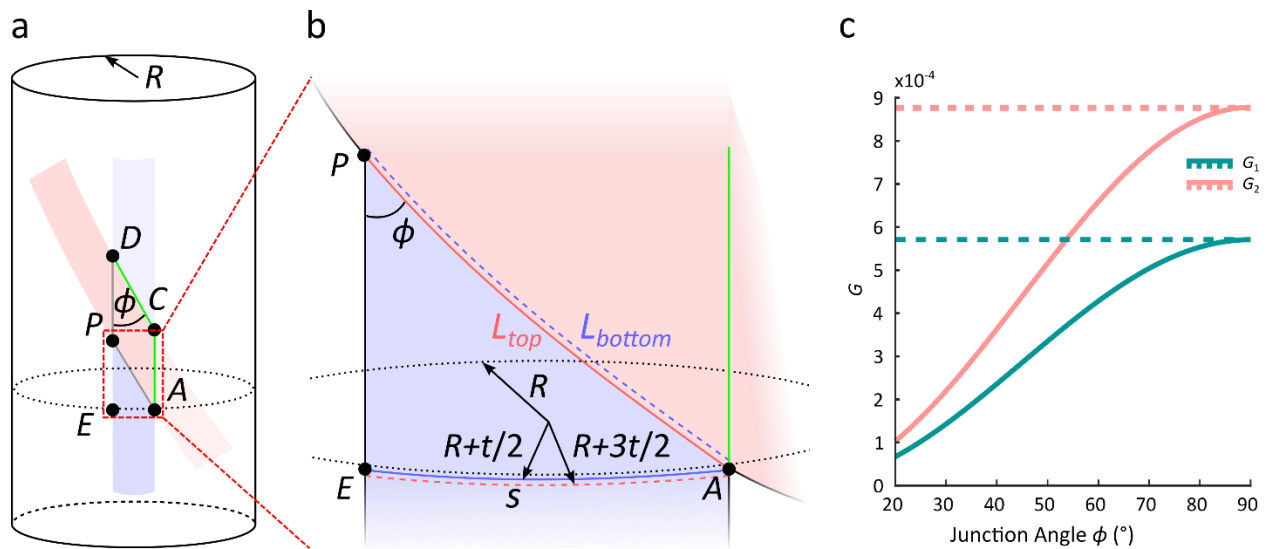a   b   c

Fig. S4. Schematics for Pre-Buckling the Junctions, related to Fig. 5

(a) Orientation of the tapes relative to the cylinder (schematic). Points and colors correspond to Fig. S2. (b) Close-up view of the bottom portion of the junction area as indicated by the dashed red box and lines. (c) Plot of G as a function of junction angle. The dashed lines represent G_{AE} for the curved segment, s, between points A and E.

Here we characterize the pre-buckle factor G discussed in the "Forced Self-Strengthening Junctions" section of the manuscript. To force the junctions into the locked conformation, we made the junctions on cylindrical surfaces with radii R_1 = 101.6 mm and R_2 = 66.0 mm. The tape–tape junctions were made by placing the first tape vertically along the axis of the cylinder, then placing the second tape on top of the first at the prescribed junction angle, ϕ, as shown in Fig. S4a. Placing the tapes on this curved surface causes the junction area to become curved. The lengths of line segments that are along the axis of the cylinder, such as $\overline{EP}$, are not curved. Segments such as $\overline{AE}$ and $\overline{AP}$ become curved according to the radius of the cylinder. This curved configuration is the relaxed state for these junctions. Under load, there will be a small, but non-zero force acting toward the restoration of the original curvature, due to the finite thickness of the tapes. For the chosen stacking order of the tapes the junction will "pre-buckle" into the locked conformation. Inverting the stacking order with the angled tape being applied to the cylinder first will cause the junction to pre-buckle into the nestled conformation. We quantify this change in length of the curve between points A and P with the pre-buckle factor, G:

$$G = \frac{L_{top} - L_{bottom}}{L_{bottom}}. \tag{S24}$$

L is the length of the curved segment between points A and P for the top and bottom tapes respectively , and $\overline{AP}$ is the length of the line segment $\overline{AP}$ when the junction is made without a pre-buckle as shown in Fig. S2a. $\overline{AP}$ is determined as $w \csc \phi$.

To determine L, we express the curve using three parametric equations as a function of u:

$$L(0 \le u \le 1) = \begin{array}{l} x(u) = (R + d) \cos\left(\frac{w}{R+t/2}u\right) \\ y(u) = (R + d) \sin\left(\frac{w}{R+t/2}u\right) \quad, \\ z(u) = 2(R + t/2) \sin\left(\frac{w}{R+t/2}\right)\cot\phi \end{array} \tag{S25}$$

where R is the radius of the cylinder, t is the thickness of the tape, w is the width of the tape, and d is the additional distance from the surface of the cylinder to the mid-plane of the tape. For the bottom tape, $d = t/2$ and the top, $d = 3t/2$. L is determined by using the length equation for parametric equations:

$$L = \int_0^1 \sqrt{\left(\frac{dx}{du}\right)^2 + \left(\frac{dy}{du}\right)^2 + \left(\frac{dz}{du}\right)^2}\, du. \tag{S26}$$

Applying eqn. S25 to eqn. S26, we get:

$$L(\phi) = \sqrt{\left(\frac{w}{R+t/2}(R + d)\right)^2 + \left(2(R + t/2) \sin\left(\frac{w}{R+t/2}\right)\cot\phi\right)^2}. \tag{S27}$$

We can now determine the pre-buckle factor, G, by applying the values of d for the top and bottom tapes to eqn. S27, we get L_{bottom} and L_{top} for eqn. S24. The result is a long expression that does not simplify, but is a function of R, t, w, and the junction angle, ϕ, which becomes apparent in Fig. S4c. The dashed horizontal line indicates the pre-buckle of segment $\overline{AE}$: $G_{AE} = (s_{top} - s_{bottom})/\overline{AE}$, which is not dependent on ϕ. At $\phi = 90°$, $\overline{AE} = \overline{AP}$, thus the pre-buckle factors for the two segments are also equal. As ϕ increases, G decreases and does go to 0 as ϕ approaches 0° because L of both tapes become equal. For all junction angles, $(1.5388 \pm 0.0005) \cdot G_1 = G_2$.

SI5 – Materials Parameters

Table S1. Constants used to model the tapes discussed, related to Figs. 3, 4, 5, 6, and 7							
Tape	Thickness (t)	Width (w)	Surface Energy (γ)	Modulus (E)	Sample Length (β)	Tensile Strength (TS)	Lap Shear Strength (LSS)
Scotch® Tape	0.058 mm (ref. S8)	12.7 mm (ref. S8)	10.3 ± 0.9 J/m^2	468 ± 8 MPa	186 ± 3 mm	23.2 ± 0.4 MPa	78 ± 22 kPa
Recluse Silk	40–80 nm (ref. S9)	5–7 μm (ref. S9)	43–52 J/m^2 (ref. S10)	15–21 GPa (ref. S9)	200 μm (ref. S7)	629 ± 190 MPa	
For the Scotch® tape material, the surface energy for the tape was experimentally determined using 90° peel tests. The modulus, TS, and LSS were determined using monotonic tensile tests.							

SI6 – Supplemental References

S1   K. Kendall, *Journal of Physics D: Applied Physics*, 1975, **8**, 1449.

S2   L. He, J. Lou, S. Kitipornchai, J. Yang and J. Du, *International Journal of Solids and Structures*, 2019, **167**, 184–191.

S3   N. Padhye, D. M. Parks, A. H. Slocum and B. L. Trout, *Review of Scientific Instruments*, 2016, **87**, 085111.

S4   K. Kendall, *Journal of Physics D: Applied Physics*, 1973, **6**, 1782.

S5   Y. Wang, X. Yang, G. Nian and Z. Suo, *Journal of the Mechanics and Physics of Solids*, 2020, **143**, 103988.

S6   R. Hertzberg, *Deformation and fracture mechanics of engineering materials*, John Wiley & Sons, Inc, Hoboken, NJ, 2012.

S7   S. R. Koebley, F. Vollrath and H. C. Schniepp, *Materials Horizons*, 2017, **4**, 377–382.

S8   3M Scotch, *3M^{TM} Scotch® Transparent Film Tape 600*, 3M, 2009.

S9   H. C. Schniepp, S. R. Koebley and F. Vollrath, *Advanced Materials*, 2013, **25**, 7028–7032.

S10 J. Zhang, S. Du, A. Kafi, B. Fox, J. L. Li, X. Y. Liu, R. Rajkhowa and X. G. Wang, *RSC Advances*, 2015, **5**, 1640–1647.